Analysis and Experimentation for the Aerial Deployment of Planetary Balloons

Christopher White[1] Shari Day[2]

[1]Jet Propulsion Laboratory, California Institute of Technology
Mail Stop 157-316
4800 Oak Grove Drive
Pasadena, CA 91109
christopher.v.white@jpl.nasa.gov

[2]Livermore Software Technology Corporation
7374 Las Positas Rd., Livermore, CA 94550
(408) 873-8178, sday@lstc.com

ABSTRACT

This paper presents the development of predictive computational models for the shock forces associated with aerial deployment of very thin, uninflated, polymer balloons. A set of three models has been developed – a multi-mass rigid body model to simulate the unpackaging and unfolding kinematics, a spring-mass model to predict the shock forces, and a large displacement non-linear finite element model to predict balloon internal stresses and strains. The models are validated through experimental deployment tests in large enclosed dirigible hangars. The work shows that the shock forces are initiated internal to the balloon and subsequently propagate away, that forces increase with separation velocity, and that there can be variability in the response for nominally identical deployments. Predictions for shock forces are consistently conservative. This work brings much insight and understanding, and predictive ability to aerial deployment, but more work is needed to confidently predict design margins.

INTRODUCTION

JPL began the MABVAP (Mars Aerial Balloon Validation) program in August 1997 to develop and validate the technology needed for a Mars superpressure balloon mission. A central feature of this research program has been to develop and demonstrate the concept of aerial deployment and inflation of lightweight polymer balloons. The interested reader is referred to references [1] and [2] for historical perspective and a summary of the goals of the program.

The analyses described in this paper were begun in summer of 2000 with the purpose of developing models that provide insight into the deployment process and ultimately that can predict the design margin of the balloon during deployment. The work reported here is restricted to shock loads of deployment, and even though aeroelastic loads such as vortex shedding and material flagging may be important subsequent to deployment, they are not addressed in this work. Prior analyses [3] by others used multi-body rigid body models to study balloon-payload oscillations, effects of tether lengths, to plan the sequencing and timing of events of events, and for studying pointing dynamics of science cameras during float conditions. A separate effort to analyze the stresses of the inflated balloon under operating conditions has been made by the authors. That analysis is comparatively straightforward and is not covered in this paper.

A prediction of the design margin implies knowledge of the failure modes. Scant experimental data existed on deployment failure modes, and what data there was had to be gleaned from on-board video footage of deployments at an altitude of 34000m, with no opportunities for inspection of the components after the deployment attempt. Schedule and fabrication costs for 10m diameter Mylar superpressure balloons make ground testing to failure quite objectionable during the MABVAP program, despite the desirability from the analysis standpoint.

Compounding the inspection and testing difficulties is the fact that balloon technology involves considerable uncertainties and variabilities in both the loading and in the component strengths, despite their apparent simplicity and reliability once in the fairly benign float environments. The exploratory nature of MABVAP meant that each balloon is a special order item and thus unique, and until recently, there were no proof tests before accepting delivery and

[1] 0-7803-7651-X/03/$17.00 © 2003 IEEE

using the balloon in a stratospheric deployment experiment. Consequently, very small initial flaws, introduced by whatever means, might go undetected until deployment, where even a mild shock force could result in catastrophic failure.

Presumably, with appropriate quality control measures and acceptance testing, balloons likely can be assured of a reasonably repeatable capacity. A challenge remains, at least potentially, in both predicting the loads and predicting the capacity during deployment. A few of the challenges for the latter include: 1) balloons have extremely large surface areas yet there is a need to capture fine details, requiring a very large finite element model, 2) the displaced shape is characterized by large displacements, small strains, and complex wrinkled shapes with a large number of equilibrium configurations, 3) uncertain or complicated material properties and ultimate strengths, with dependence on temperature, humidity, directionality, and possibly strain rate, and 4) extremely complicated energy loss mechanisms. It is likely that not all of these challenges will need to be met, once the most relevant failure mode or modes can be identified.

Regardless of how difficult it may be to achieve in practice at this point, we retain the excellent objective of predicting the design margin and attempt to solve the problem by solving the component problems: determine the deployment loads, determine the internal stresses due to these loads, then determine the failure modes and capacity.

The remainder of the paper is organized as follows. We continue with a discussion of the aerial deployment, the components comprising the flight train, and the methods for packing and stowing the balloon. Next, we present the two models for estimating the internal shock force. One model predicts the kinematics of the flight train as the balloon is pulled free of its storage container, and a second model predicts the forces that result as the balloon snaps taut at the end of the deployment. The paper continues with a section devoted to the experimental program of ground-based deployments used to validate the models. A final section of the paper describes a pilot study using a nonlinear finite element analysis. The paper concludes with recommendations for future work.

FLIGHT TRAIN AND PACKAGING SCHEME

The balloon and other elements of the system are packaged in the aeroshell for entry. The deployment sequence (see Figure 1) includes 1) separation of the aeroshell and heatshield and parachute deployment, 2) after reaching terminal descent, the balloon is deployed from its container, 3) inflation commences from the bottom, 4) balloon completely fills, and inflation system and parachute are jettisoned.

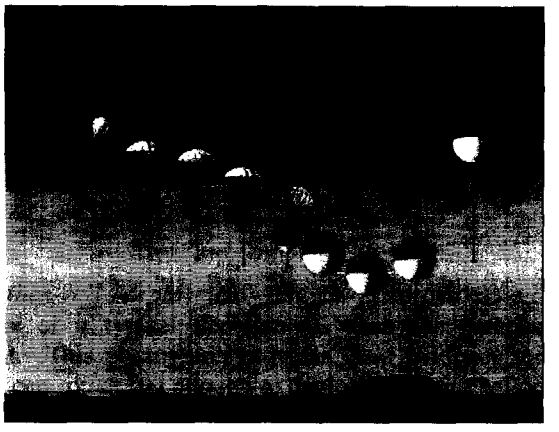

Figure 1 Artist's rendition of proposed entry and aerial deployment sequence for a balloon mission on Mars.

The components comprising the flight train in stratospheric deployment tests is similar to what would be expected for an actual mission. It should be noted that the purpose of flight testing in the stratosphere is to maintain a similar density to the Martian atmosphere (~ 0.01 kg/m^3); the Martian gravity is 3.72 m/s^2. The flight train, shown in Figure 2, consisted of the following components:

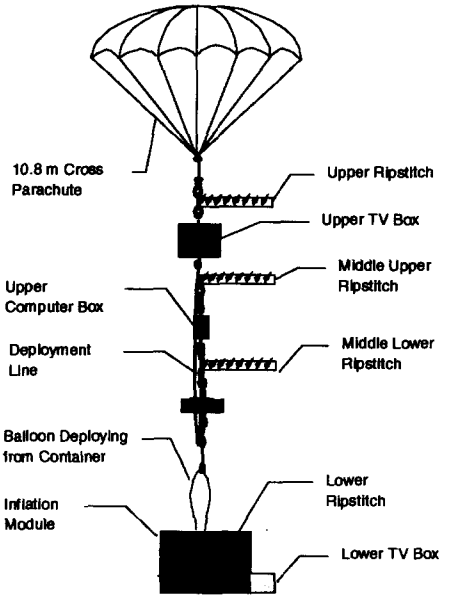

Figure 2 Schematic of flight train for stratospheric deployment and inflation tests.

Descent Parachute—10.8m cruciform parachute

Ripstitch—force limiting device constructed by folding webbing in the middle and stitching with rows of thread. Number of rows determines the ripping force.

TV Cameras and Signal Conditioners— lightweight boxes housing miniaturized downward looking video camera and accelerometer signal conditioning equipment.

Table 3 Predicted kinematics for an identical system using the two packing schemes.

Method	Deployment time τ (s)	Separation Velocity, ΔV (m/s)
Fold-then-roll	1.42	21.5
z-fold	1.15	26

DEPLOYMENT SHOCK FORCES

A model of the entire flight train is constructed based on the geometry of the fully deployed balloon immediately prior to the shock event. The deployed but uninflated balloon is discretized into a number of nonlinear springs with associated masses, and mass are added for each important component of the flight train and joined with springs of appropriate stiffness. The ripstitch force-limiting devices are modeled with special inelastic elements. The spatially discontinuous initial velocity conditions are imposed based on the deployment kinematics simulations. The equations of motion are simple and can be written by inspection for any discretization of the balloon. The entire system of equations is solved with a custom MATLAB computer program script file.

Balloon model—Discrete masses representing the balloon are calculated using tributary areas. Masses of end fittings are lumped in with the tributary mass. The upper fitting has a mass of 0.3kg and the lower fitting a mass of 0.4kg. Total balloon mass for the 10m diameter Mylar sphere is 6.88 kg.

Stiffness of the balloon under axial loads is a stiffening nonlinear function of stretch. To determine the correct nonlinear stiffness, careful experiments were performed on two different balloon designs by fixing one end of the balloon and slowly pulling the other end while measuring displacements. The measured load-deflection curves for the loaded end are shown in Figure 5.

A simple power law expression was fit with least squares to the pull test data to establish an analytical representation of the stiffness that was valid for the entire balloon. The balloon was assumed to be elastic meaning that loading and unloading takes place along the same curve. Displacement compatibility and equilibrium were used to derive the correct spring stiffness for each spring in the discretized model.

Ripstitch Model—The ripstitch is assumed to behave as an elastic-perfectly plastic element. Most ripstitch elements have a failure load which increases with tear distance because the number of rows of stitching increases as one moves from the end. An example of measured ripstitch force is shown in Figure 6. The staircase profile of failure load with tear distance is handled with a simple lookup table. Internal force in the ripstitch is zero if the adjacent masses have negative relative velocity or if the ripstitch is slack. Otherwise, the ripstitch is assumed to be tearing and the internal force is given by the force level associated with the total torn distance.

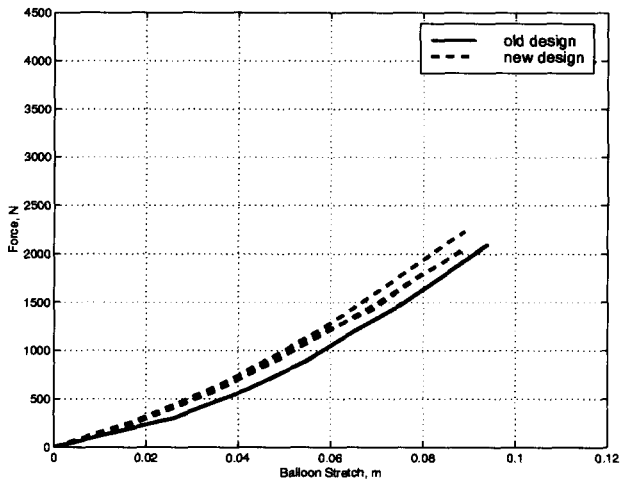

Figure 5 Measured load-deflection curves for two 10m diameter balloons of slightly different end cap designs.

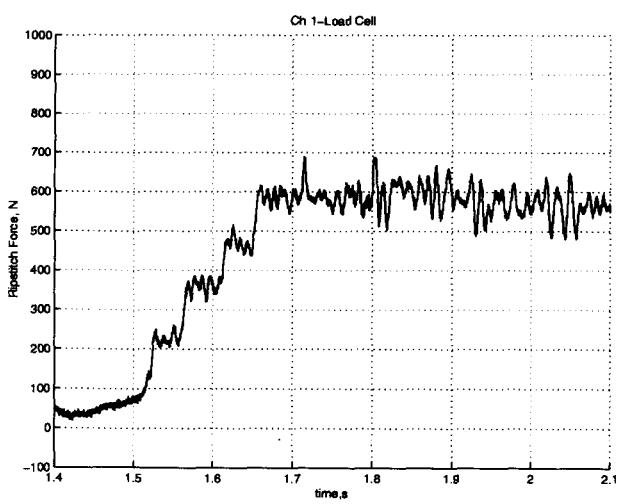

Figure 6 Ripstitch forces measured during deployment test shows the different force levels associated with different number of rows of stitching.

The hysteresis in the ripstitch response is handled by storing the instantaneous total ripped distance in a global variable that is updated within the ripstitch computation function. Small modifications were required to the built-in MATLAB Runge-Kutta ODE solver to be sure that the required mid-interval evaluations of ripstitch force do not erroneously update the total ripped distance.

Shock Force Predictions—The spatial and temporal evolution of internal balloon forces is shown as a waterfall plot in Figure 7, for a representative deployment event.

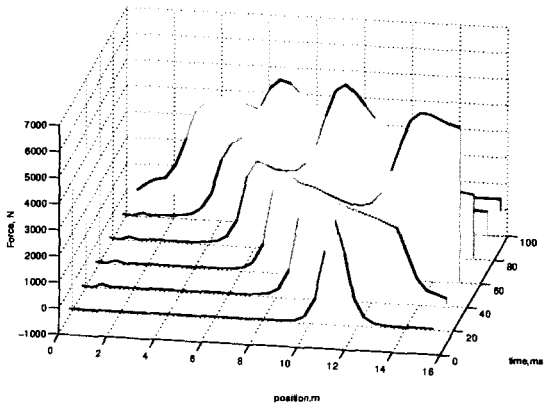

Figure 7 Evolution of internal shock forces. Force is on the vertical axis, position along the balloon is on the left-to-right axis, with the top of the balloon at far left, and time is on the front-to-back axis.

Numerous simulations have been run and the results have led to some fundamental understandings of the deployment forces:

1. As Figure 7 makes clear, the shock force begins internal to the balloon and must travel through the balloon before it reaches the ripstitch.
2. The peak internal force is actually due to the wave being reflected and occurs at balloon ends, not at the source of the shock.
3. The peak internal force is much greater than the limiting force of the ripstitch.
4. The peak internal forces are largely insensitive to mass of the deployment module DM.

Other conclusions that were reached through parameter studies and in the process of planning experiments include: a strong dependence on the internal shock forces with the separation velocity ΔV, a relationship between demand in specific ripstitches and the assumed location of the shock initiation, and while the internal shock forces are largely insensitive to the mass of the DM, the shock forces show a sensitivity to small masses above the balloon.

HANGAR DROP TESTS

Outline

Data was gathered to validate the simulation models through an extensive ground-based testing program. Some of the tests were relatively simple, such as component load-deflection tests or small-scale deployment tests in the JPL Aerobot lab. The more complex and interesting tests involved full-scale deployments in large dirigible hangars in Tillamook, OR and NASA Ames Research Center in Mountain View, CA. These mammoth facilities are the only facilities that can accommodate the required balloon deployment lengths while simultaneously providing a wind-free environment.

The standard sensor layout included DC accelerometers on the end fittings of the balloon itself, on the DM, and sometimes above the balloon, and load cells immediately above and below the balloon. Typically, video recording was also made from several cameras simultaneously, providing different views of the deployment.

The typical hangar configuration included a 10m diameter 12μm thick Mylar balloon in the fold-then-roll configuration, a 23kg DM, ripstitches immediately above and below the balloon, and various lightweight equipment boxes above the balloon that are part of the flight train during stratospheric deployments. Where noted, additional tests were performed using an external load line in parallel with the balloon.

The effects of the parachute were mimicked by suspending the entire flight train from a number of latex tubes fixed to the roof of the facility. By altering the force provided by the tubing, one can alter the separation velocity ΔV of the deployment.

Four separate test sessions took place as described below.

August 2000, Tillamook—Static deployment experiments with flight train firmly attached to roof. Data provided measurements of deployment time, of ripstitch nominal failure loads, and of separation velocity ΔV by integration of accelerometer. ΔV=17m/s was achieved. Measurements validate concept of shock force modeling through velocity initial conditions.

July 2001, NASA Ames—Small number of experiments to observe deployment with an external load line and to check improved data acquisition system. Debut of new latex tubing suspension system. Experiment provides measurements of ΔV and forces above and below balloon.

October 2001, NASA Ames—Extensive set of drop tests with latex tubing suspension system, to gather comprehensive data for model validation, and to investigate strength margin of balloon by increasing ΔV. Experiments achieved ΔV ranging from 14 m/s to 28 m/s. Additional drops with external load line, and with z-fold packing.

April 2002, NASA Ames—Drop tests to observe deployment with external load line, observe deployment of pumpkin balloon with z-fold packing, and to perform proof-testing of balloons intended for stratospheric deployment.

Summary of Measurements

The most complete and reliable set of measurements was obtained from October 2001 tests. The highlights of those measurements can be synthesized into a few graphs.

Peak acceleration as a function of ΔV is shown in Figure 8. The measured ΔV was determined by integrating the accelerations measured on the DM and on the equipment box above the balloon and subtracting. The data generally show an increase in response with an increase in ΔV, and generally show that accelerations at the top fitting are larger than those at the bottom. Test conditions for the two deployments at ΔV=20 m/s were nominally identical, so the factor of more than two scatter in the measured data is surprising.

Peak force measured in the tethers above and below the balloon end fittings is shown in Figure 9. Again, there is an increase in response with increasing ΔV, and the peak forces measured above the balloon are larger than those below the balloon. In contrast to the peak accelerations, the peak forces for the two ΔV=20 m/s deployments are nearly identical. The lower than expected forces in the ΔV=28 m/s deployment is thought to be caused by the failure of a knot in the flight train.

Although the responses fit a general trend of increasing with increasing ΔV, the data clearly shows that variabilities are possible from test to test. This is thought to be a natural attribute of the uncontrolled deployment process. Angular displacement and misalignment of the end fittings during the shock is a possible explanation for the difference seen in Figure 8, but additional investigations have not been made to date to confirm this hypothesis.

It remains to be seen to what extent these variations are inherent in the packing and deployment process. It is possible that other conditions could be the cause: variations in the stretched surgical tubing, the presence of initial slack in the stowed flight train, the presence of the sensors themselves, the cabling, or even incomplete understanding of the basic physics.

More detail regarding the variabilities is seen in Figure 10 and Figure 11. Figure 10 shows acceleration measurements made for tests 'D' and 'D1'. The signals are measured on the upper fitting of the balloon, and on the lightweight signal conditioner box just above the balloon. One sees substantial agreement in waveform between locations on Drop D1, but disagreement on drop D. In addition, the waveforms disagree between the two drops. Figure 11 compares the signals on the lower fitting.

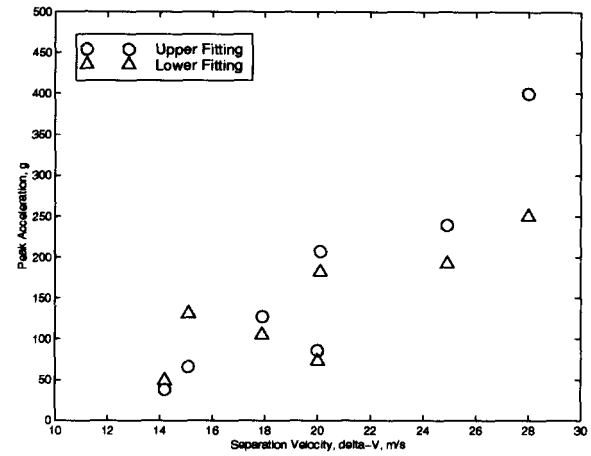

Figure 8 Peak acceleration measured on the balloon upper and lower end fittings as a function of measured ΔV.

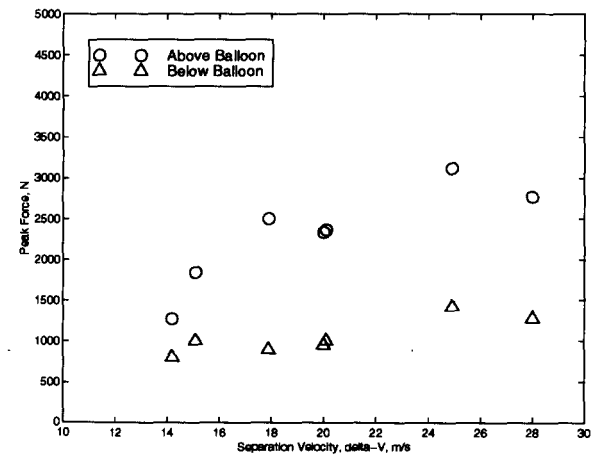

Figure 9 Peak force in tethers above and below balloon versus ΔV.

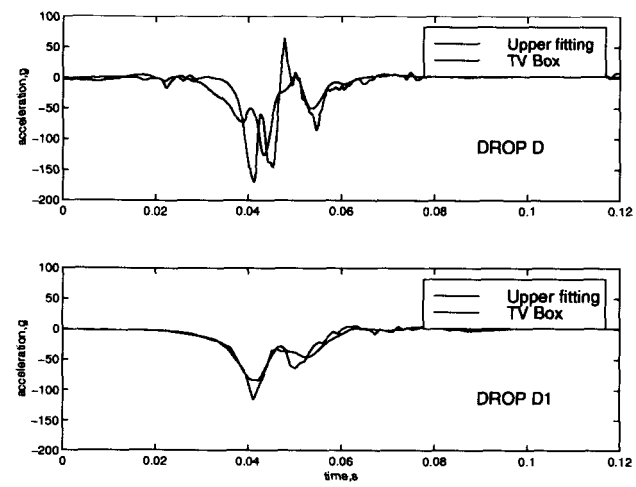

Figure 10 Comparison of upper fitting signals. Drop D = 18 m/s, Drop D1 = 20 m/s.

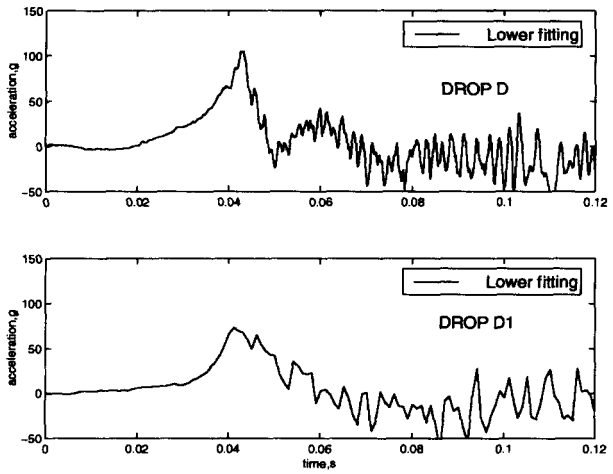

Figure 11 Comparison of lower fitting signals. Drop D = 18 m/s, Drop D1 = 20 m/s.

Comparison to Model

Each deployment experiment was simulated in the shock force program using the most accurate input conditions possible. Test and analysis data are compared in Figure 12, where it can be seen that analysis consistently over-predicts the test measurements.

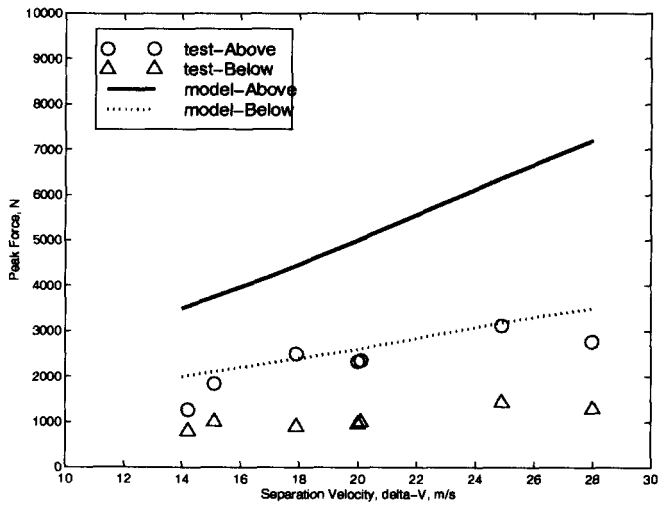

Figure 12 Comparison of peak deployment forces above and below balloon from simulation (lines) and test (points).

FINITE ELEMENT MODEL

A pilot study was undertaken to analyze the stresses due to a 4500N static load applied to a 1/8th symmetry model of the uninflated balloon in the axial direction. The LS-DYNA3D finite element analysis program [4] was chosen because of its excellent capabilities for this class of problem. The analysis is useful for predicting strength and mode of failure, and could be used as needed to guide design changes for strengthening the balloon. The same model was also used for analyzing the balloon under internal pressure loads, a much simpler analysis.

Shell and membrane finite elements were used to construct a model using the reference geometry of a nominally spherical 10m diameter shape built up of flat gores. The model is depicted in Figure 13. This reference geometry was the only geometry known for the balloon, yet it was very far from the equilibrium shape sought for the static axial load. Attempts were made to define the geometry in a stress-free state that was closer to the deployed shape, but they were abandoned due to concerns that distortion would be introduced. Instead, the entire configuration was computed as it moved from spherical to tube-like under axial load.

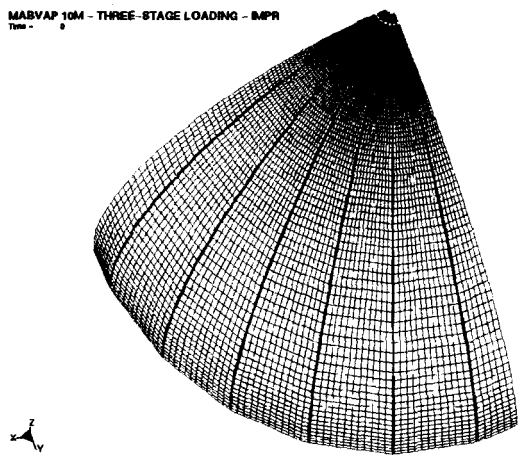

Figure 13 View of FE mesh in reference configuration. Model has 13400 nodes, 13200 elements, and 80400 DOF.

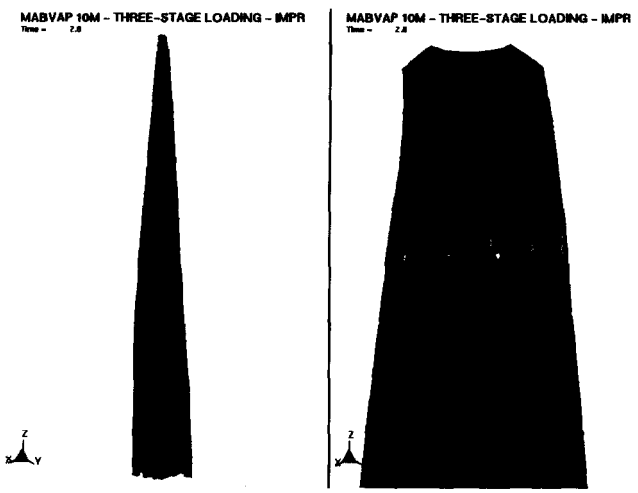

Figure 14 Deformed mesh of balloon due to a small preload, showing the collapsed configuration, with details at the top fitting.

The response was computed using an elastic, geometrically nonlinear transient solution method. A nominal preload was applied and held constant in order to move the balloon away from the reference configuration into the axial shape of the deployed but uninflated balloon. After the system picked up some axial stiffness, the load was gradually increased to the full 4500N value.

A plot of the collapsed configuration at preload is shown in Figure 14. The stiffening ring buckles into two full waves per 90° segment. The doubler region and balloon fabric form folds. Folds in the doubler are influenced by the ring deformation; folds in the film show some influence from the gore and seam pattern.

A contour plot of axial-direction stress is shown in Figure 15 and indicates two stress hot spots at the crests of the buckled waves in the stiffening ring. Peak stress in the doubler is about 200 MPa. At the doubler-film transition, stress is about 140 MPa in the film. Figure 16 and Figure 17 show stress as a function of position at cross-sections through the doubler and film, respectively. The effect of the hard points generated by waves in the ring is apparent in Figure 16. In the film, at a distance away from the ring, the stress variation starts to conform more to the gore pattern, with stress higher at panel centerlines. A stress of 140 MPa is above the material's yield stress at room temperature, so if accurate stress distributions around the stress concentrations are required, a nonlinear material model should be used. This would be a fairly routine option in LS-DYNA.

The analysis reproduces many aspects of structural response witnessed in the balloon load deflection measurements shown in Figure 5: the stiffening ring buckles into a circumferential wave pattern, the balloon film creases and forms pockets, and the load deflection curve is a stiffening nonlinear function. Agreement between test and simulation load-deflection curves is remarkably good, as shown in Figure 18. No attempt was made to estimate the balloon's strength from this analysis, as the failure mode is unknown.

This model uses a fabric material model for the film, self contact on the balloon body, and additional contact conditions at the symmetry planes and upper fitting where load is applied. The balloon film is extremely thin, at just 12 microns. It proved to be difficult at first to get a stable, credible solution. The material model required adjustments, and contact violations caused simulations to crash. Many different loading strategies were tried. Simulations that successfully reached final load all show similar results, regardless of the load history. Thus, results are repeatable and the modeling effort was deemed successful, irrespective of the difficulties encountered.

Simulations recently run using a new contact algorithm in the latest release of LS-DYNA are very stable, suggesting that this analysis technique may indeed be a viable design tool. Analysis run time was about 10 hrs of cpu time per 1 second simulation time on a UNIX workstation. Each 4 second simulation took about 20 hours to run, using two processors.

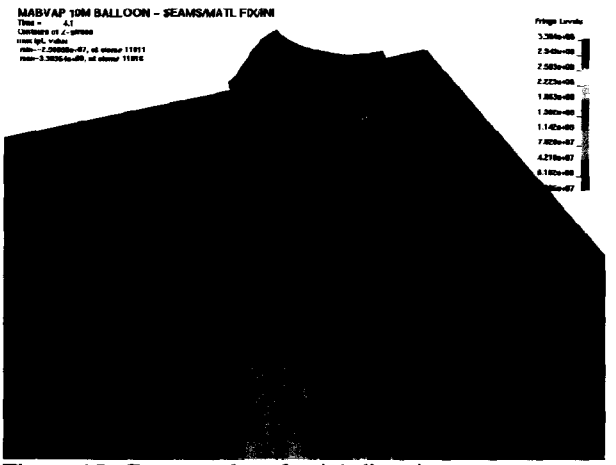

Figure 15 Contour plot of axial-direction stress.

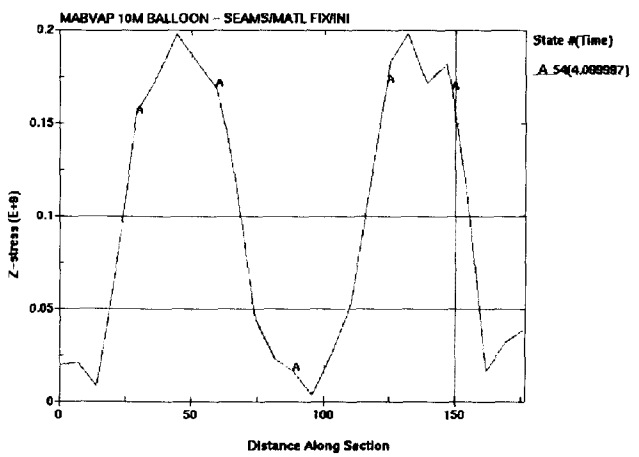

Figure 16 Stress variation around circumference in doubler near stiffening ring.

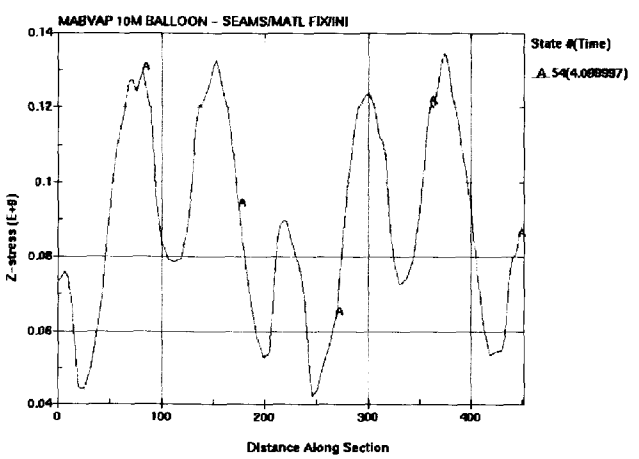

Figure 17 Stress variation around circumference in film near doubler.

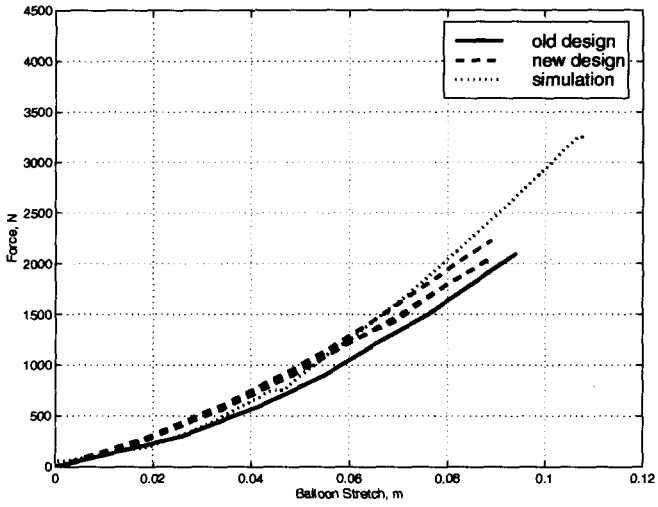

Figure 18 Comparison of FE simulation results to load-deflection measurements shown in Figure 5.

CONCLUSIONS

These analyses and experiments have provided the MABVAP team a greatly improved understanding of the mechanics of deployment. Among the chief results are that the shock force has its genesis within the interior of the balloon, which leads to the very important conclusion that ripstitch can only mitigate the shock force after it has propagated outside the balloon. It then follows that the maximum internal balloon force is not limited to the tearing strength of the ripstitch. Another important result is that separation velocity ΔV has been established as a key parameter in determining the shock force.

The two deployment models developed in this research are fairly simple and qualify as practical design and analysis tools. They can be used to discern between design alternatives, such as fold-then-roll packing or z-fold, and can be used to specify the amount of ripstitch required above and below the balloon. The finite element model, which uses 80400 DOF, is a challenging and relatively costly analysis but can be used to quantify stresses in the balloon and be used to assess merits of proposed design modifications such as selective strengthening of doubler components, or the introduction of load tapes.

Although the required analysis tools are now available, the goal of predicting the design margin of the balloon system during deployment remains a difficult challenge. Additional experiments, possibly including stratospheric deployments, would be required to understand the dominant failure modes. Stratospheric deployments with a full complement of sensors would be required to determine the in-service loads in the stratosphere. Depending on the failure modes identified, specialized material testing may be required.

ACKNOWLEDGEMENT

The research described in this paper was carried out by the Jet Propulsion Laboratory, California Institute of Technology, and its collaborators under a contract with the National Aeronautics and Space Administration. The discussions and contributions of V. Kerzhanovich and J. Hall are greatly appreciated. The assistance of M. Pauken, B. McDonald, H. Cooper, T. Lachenmeier and S. Mooney in performing the experiments is gratefully acknowledged.

REFERENCES

[1] V. Kerzhanovich, J. Cutts, A. Bachelder, J. Cameron, J. Hall, J. Patzold, M. Quadrelli, A. Yavrouian, J. Cantrell, T. Lachenmeier, M. Smith. "Mars Aerobot Validation Program," *Paper AIAA-99-3853, AIAA Balloon Technology Conference, 1999.*

[2] V. V. Kerzhanovich et al, "Breakthrough in Mars Balloon Technology", Paper PSB1-0076-02, *34th COSPAR Scientific Assembly, Houston, TX, USA, 10-19 October, 2002.*

[3] M. Quadrelli, J. Cameron, V. Kerzhanovich, "Multibody Modeling and Dynamics of Parachute and Balloon Flight Systems for Planetary Exploration," *Paper AIAA 2001-2026, 16th AIAA Aerodynamics Decelerator Conference, Boston, MA, 2001.*

[4] J. O. Hallquist, LS-DYNA Keyword User's Manual, LS-DYNA Version 960, Livermore Software Technology Corporation, Livermore, CA, March 2001.

[5]

BIOGRAPHIES

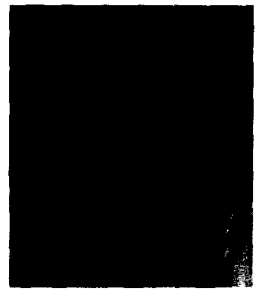

Dr. Christopher White is a Senior Engineer in the Interferometry and Large Optical Systems Section. His areas of interest include computational and experimental investigations for structures and structural dynamics, structural performance of space-born optical systems, and analysis and behavior of thin-film structures. Previous employers include Exponent Failure Analysis Associates in Menlo Park, CA, and Structural Dynamics Research

Corporation in San Diego, CA. He holds a Bachelor's and a Master degree in civil engineering from George Washington University, and a PhD in civil engineering from Cornell University. He is a registered Professional Engineer in CA.

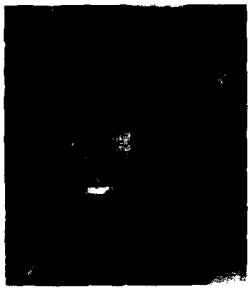

Shari E. Day, PE, is a registered Professional Engineer in California. Ms. Day has 17 years experience in structural design and analysis, including 15 years at Exponent Failure Analysis in Menlo Park, California, performing structural investigations and stress analysis of components and structures by the finite element method. Currently, Ms. Day is a consultant for Livermore Software Technology Corporation specializing in dynamic numerical analysis. Ms. Day has a BSCE from Virginia Tech and an MSCE degree in Structures from the University of Colorado, Boulder.